Biointerface Research in Applied Chemistry
Platinum Open Access Journal (ISSN: 2069-5837)

Article
Volume 12, Issue 6, 2022, 8057 - 8069
https://doi.org/10.33263/BRIAC126.80578069

Adsorption of Hydrogen Sulfide (H_2S) from Municipal Solid Waste by Using Biochars

Tengku Nuraiti Tengku Izhar [1,*], Goh Zhi Kee [1], Farah Naemah Mohd Saad [2], Shayfull Zamree Abd Rahim [3], Irnis Azura Zakarya [4], Mohd Rizam Che Besom [5], Mursyidul Ibad [6], Achmad Syafiuddin [6]

1 Faculty of Civil Engineering Technology, Universiti Malaysia Perlis (UniMAP), Perlis, Malaysia
2 Water Research & Environmental Sustainable Growth (WAREG), Universiti Malaysia Perlis (UniMAP), Perlis, Malaysia
3 Geopolymer & Green Technology, Centre of Excellence (CEGeoGTech), Universiti Malaysia Perlis (UniMAP), Perlis, Malaysia
4 Environment Research Group (SERG), Centre of Excellence Geopolymer and Green Technology (CEGeoGTech), Universiti Malaysia Perlis (UniMAP), Perlis, Malaysia
5 E- Idaman Sdn. Bhd. Wisma Idaman, Alor Setar, Kedah, Malaysia
6 Department of Public Health, Universitas Nahdlatul Ulama Surabaya, 60237 Surabaya, Indonesia
* Correspondence: nuraiti@unimap.edu.my (T.N.T.I.);

Scopus Author ID 57189071410
Received: 5.10.2021; Revised: 5.11.2021; Accepted: 8.11.2021; Published: 5.12.2021

Abstract: The emission of hydrogen sulfide (H_2S) from municipal solid waste is one of the environmental issues that raised the public's attention and awareness. Exposure to H_2S that brings a foul smell of rotten eggs will cause headaches, irritation, dizziness, fatigue, and even death if the concentration of H_2S is too high. The study's goals are to investigate the properties of biochars made from rice hulls, banana peels, and sawdust; to compare the biochars' physical and chemical properties; and establish the H_2S removal efficiency of the three biochars. Biochars derived from rice hull (RHB-500), banana peel (BPB-550), and sawdust (SDB-500) by pyrolysis were used as the adsorbents. The biochar yield, pH, ash content, surface functional group, and morphology of the biochars produced were investigated. In this study, H_2S was synthesized by mixing food waste and soil in the experimental column. The H_2S produced was reduced by the adsorption method. The removal efficiencies of H_2S for each biochar were determined by allowing the synthetic H_2S to flow through the two columns that were packed with sand (act as control) and biochars, respectively. All biochars were alkaline, and BPB-550 had the highest pH, followed by SDB-500 and finally RHB-500. The order for removal efficiency of H_2S (>94%) is BPB-550 > SDB-500 > RHB-500. Overall, the biochars derived from biomass had a strong ability to act as the adsorbents for H_2S removal.

Keywords: municipal waste; environmental protection; hydrogen sulfide; biochars; adsorption.

1. Introduction

Adsorption is a widely used technology for desulfurization since it is not as complex as other methods, and the removal efficiency is considered high [1]. Generally, adsorbents are low-cost materials from the industry like by-products and waste materials [2]. Adsorbents with high selectivity toward target compounds and high adsorption capacity are preferred. Traditional adsorbents, such as natural and synthetic zeolites, have recently gotten a lot of attention. Zeolites are microporous crystalline solids created structurally by a combination of

SiO_4 and AlO_4 tetrahedra sharing a vertex, and they have been widely utilized in the petrochemical sector as catalytic materials and adsorbents, as well as water softeners in detergents [3]. Biochar is a solid product derived from biomass by undergoing pyrolysis [4]. Biomass pyrolysis is a method of thermal degradation of biomass raw materials without the need for air or oxygen, and it is used to generate solid (biochar), liquid (tar and other organic matter), and gas products [5,6]. Biochars can be derived from broiler litter, sawdust, and furfural residue [7]. They are also biochars from the banana pseudostem and fruit bunch stem [8]; and camphor, rice hull, and bamboo to produce the biochars [9]. Daily manure and rice husk were used to produce biochars in the research that was done [10].

Odorous gaseous released from landfills is becoming a global issue for both the general population and the specialized group in the world. The major odorous gas is hydrogen sulfide (H_2S). H_2S is a colorless, flammable gas with a characteristic "rotten-egg" stench that is prevalent in industrial operations such as petroleum refining, natural gas processing, and wastewater treatment [11]. H_2S has a recommended Immediately Dangerous to Life and Health (IDLH) value of 100 ppm because it is an irritant to respiratory linings and a chemical asphyxiant, and prolonged exposure can be deadly. H_2S impurities in gas streams are very corrosive to pipes and other equipment, in addition to being hazardous to people in high quantities [12]. Long-term exposure to a low concentration of H_2S could lead to symptoms like dizziness, headache, and breathing difficulties [13]. H_2S removal methods are adsorption onto various media, chemical scrubbing, and biological desulfurization. In this study, the adsorption method was used to reduce the concentration of H_2S while biochars acted as the adsorbents.

To create a cleaner environment, effective methods for removing H_2S from static and mobile sources must be established [14]. The study aims to produce and investigate the characteristics of biochars derived from rice hull, banana peel, and sawdust. Next is to determine and compare the physical and chemical characteristics of the biochars and to determine the removal efficiency of H_2S by the three different biochars. The biochars were generated at different pyrolysis temperatures under the pyrolysis condition. High pH could favor the dissociation of oxygen-containing groups of biochars during the decontamination of pollutants [15]. Therefore, biochars with higher pH were desirable. This study developed an adsorption process that is more economical and effective in removing the H_2S from municipal solid waste landfills. The process will be simple, and the materials used are easily accessible. Therefore, the landfill operators can apply the process to their landfill sites since H_2S is toxic and will cause death if the concentration of H_2S is extremely high. Workers working at the landfill and sensitive receptors nearby have a high risk of being exposed to the H_2S. The exposure of landfill workers and sensitive receptors may be minimized by using the technique proposed in this study, and therefore the potential health danger to them could be decreased as well.

2. Materials and Method

2.1. Preparation of biochars.

Adsorption methods for removing H_2S generally employ mesoporous materials (activated carbon), which are also frequently used as catalysts due to their surface chemistry, high degree of microporosity, and developed surface area (which may reach 1000 m^2/g). This material may have crystalline and/or amorphous structures at the macro and nanoscales, but they may be further modified to modify their physicochemical characteristics, therefore

increasing their adsorption ability against the target molecules [16]. The catalyst, also known as biochars in this research, was produced from three different feedstocks: rice hull, banana peel, and sawdust. All feedstocks were cut into smaller pieces for easier handling, washed, and dried under 100°C in the oven for 24 hours. Using a crusher and wet blender, the dried pieces were then grounded and sieved for 2-mm using a sieve. Then the dried pieces were placed in crucibles with lid and pyrolysis at 400°C, 450°C, 500°C, 550°C, and 600°C in a furnace under a limited oxygen atmosphere respectively for 4 hours while the heating rate was set at 10°C / min initially. After that, the heated pieces will be cooled to the room temperature of 27°C [9]. Finally, the biochars were sieved for 0.2 mm by using a sieve.

2.3. Characterization of biochars.

The pH level for the biochar was determined by using a pH meter. 1g of biochar sample was dissolved in the distilled water with a ratio of 1:40 (biochar: deionized water). The mixture was stirred for 10 minutes and equilibrated for 30 minutes [17]. The percentage of biochar yield was determined by using the ratio of the mass of the sample after the pyrolysis to the mass of the sample before the pyrolysis [18]. The ash content of each biochar was determined by placing the biochars sample in the crucibles and heating it in the furnace at 800°C for 2 hours [10]. After the heating, samples were allowed to cool to room temperature and weight. The surface functional group for three different biochars and feedstocks was determined using the Fourier Transform Infrared (FTIR) Spectroscopy RXI Spectroscopy. The samples were scanned between the wavelengths ranging from 4000 to 650 cm^{-1} [19]. Scanning Electron Microscopy (SEM) was used to study the surface morphology of the feedstocks and biochars. The samples were placed on a double-sided platinum coating tape and observed under the magnifications of 1000x with the acceleration voltage of 10 kV [20].

2.4. Synthesis of hydrogen sulfide (H_2S).

Synthetic MSW was prepared by mixing the fruit waste, vegetable waste, rice, rotten eggs, and soil in a column (inner diameter = 145 mm; height = 800 mm). The MSW was synthesized according to the schematic diagram as shown in Figure 1.

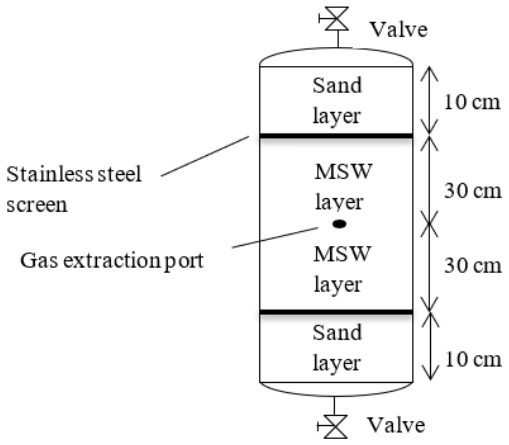

Figure 1. Schematic diagram of synthetic H_2S.

Sand acted as a leachate drainage layer. Stainless steel screen was placed between the sand and waste layers to prevent the sand from filling the voids of the MSW layer. The column was sealed with aluminum foil and wrapped with a black plastic bag to prevent the MSW from sunlight and synthesize an anaerobic condition.

2.5. Adsorption of hydrogen sulfide (H_2S).

To determine the removal efficiency of H_2S by biochars, the laboratory scale apparatus was set up according to the schematic diagram as shown in Figure 2. There were two columns, Column B and Column C (inner diameter = 145 mm; height = 800 mm) packed with sand, which acts as a control, and rice hull biochar, respectively.

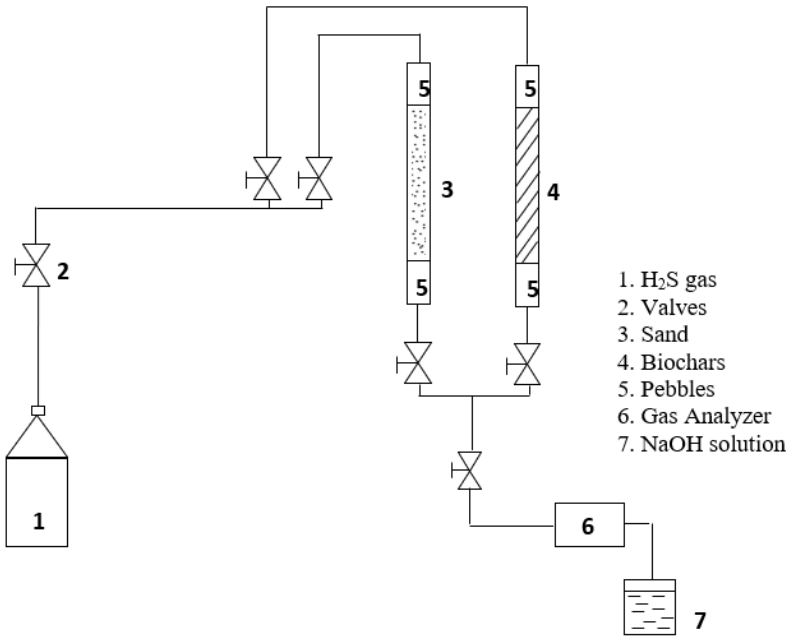

Figure 2. The schematic diagram for the laboratory-scale apparatus setup.

The initial concentration of synthetic H_2S was detected by using Gas Analyzer (GA5000). Then, the synthetic H_2S in Column A was supplied through the inlet. The adsorption zone travels from the top to the bottom of the column or fixed bed [21]. After the flow passed through the adsorption column, the final concentration of H_2S was detected and tabulated. Sodium hydroxide (NaOH) solution was prepared to prevent the excess H_2S from releasing into the atmosphere. The procedure was repeated by replacing the rice hull biochar with banana peel biochar and followed by sawdust biochar. Each run of the experiment was eight hours, while the concentration of H_2S was monitored every one hour.

3. Results and Discussion

3.1. Characterization of biochars.

Thermochemical conversion occurs in an anaerobic environment during pyrolysis. A high temperature provided by an external source causes chemical compounds to break down into smaller molecules, which is a complicated process. During the procedure, an endothermic reaction takes place [22]. Table 1 shows the pH value of biochars derived from rice hull, banana peel, and sawdust at 400°C, 450°C, 500°C, 550°C, and 600°C.

Table 1. Characteristics of biochars at different pyrolysis temperatures.

Biochar	Temperature		Colour	pH level	Biochar Yield (%)	Ash Content (%)
Rice Hull	400 ^{0}C	RHB-400	Black	8.06	41.93	-
	450 ^{0}C	RHB-450	Black	8.78	38.76	-
	500 ^{0}C	RHB-500	Black	9.55	36.45	48.07
	550 ^{0}C	RHB-550	Grey	9.60	32.54	-
	600 ^{0}C	RHB-600	Grey	9.74	30.12	-
Banana Peel	400 ^{0}C	BPB-400	Black	10.50	39.52	-

Biochar	Temperature		Colour	pH level	Biochar Yield (%)	Ash Content (%)
	450 ^{0}C	BPB-450	Black	10.58	37.65	-
	500 ^{0}C	BPB-500	Black	10.83	35.86	-
	550 ^{0}C	BPB-550	Black	11.53	33.14	26.42
	600 ^{0}C	BPB-600	Grey	11.59	28.18	-
Sawdust	400 ^{0}C	SDB-400	Black	7.55	29.36	-
	450 ^{0}C	SDB-450	Black	9.53	27.55	-
	500 ^{0}C	SDB-500	Black	9.77	25.76	19.79
	550 ^{0}C	SDB-550	Grey	10.16	24.02	-
	600 ^{0}C	SDB-600	Grey	10.17	22.65	-

From the results, all biochars produced are alkaline. Pyrolysis temperature affects the pH level of biochars significantly. The optimal temperature for the calcination process is to produce a good removal performance for H_2S gas [23]. As the pyrolysis temperature increases, the oxygen-containing functional groups' decrease; thus, the acidic functional groups reduce, leading the biochars to be more alkaline [20]. A high pH level could enhance the dissociation of H_2S and thus has a higher removal potential of H_2S concentration [24]. According to Table 1, overall, rice hull biochar possessed the highest biochar yield percentage. Sawdust biochar had the lowest lignin content in its feedstock, showing the lowest biochar yield percentage [18]. As the pyrolysis temperature increases, the devolatilization rate decrease, the carbonization process could be complete; thus, the thermal decomposition of lignin and hemicellulose increases, resulting in the decrease of biochar yield [17,25,26]. Pyrolysis will contribute to high ash content [27]. RHB-500 had the highest ash content (48.07%) compared to the other two types of biochars. Higher ash content means the combustion of C is complete [28]. Since RHB-500 possessed the highest ash content, rice hull biochar might have the highest mineral content.

3.2. Surface functional group.

The determination of the functional groups contained in feedstocks and biochars, Fourier Transform Infrared (FTIR) spectroscopy was conducted. Figure 3 and Figure 4 present the FTIR spectra of the feedstocks and biochars scanned between the wavelengths of 4000–650 cm$^{-1,}$ respectively.

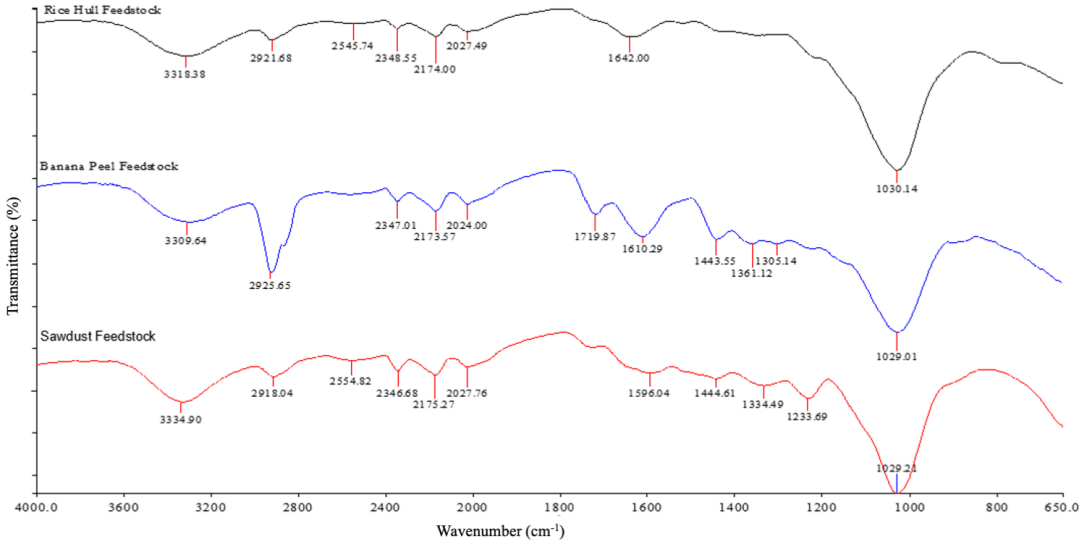

Figure 3. FTIR spectra of each feedstock.

Table 2 and Table 3 presented the possibilities of the presence of functional groups found in different samples. Table 2 shows that the wavenumber for the rice hull, banana peel, and sawdust feedstocks range between 3318.38–1030.14 cm^{-1}, 3309.64–1029.01 cm$^{-1,}$ and

3334.90–1029.21 $cm^{-1,}$ respectively. On the other hand, from Table 3, RHB-500, BPB-550, and SDB-500 gave a wavenumber range of 3637.74–797.21 cm^{-1}, 3119.64–684.84 $cm^{-1,}$ and 3336.78–1187.64 cm^{-1} correspondingly.

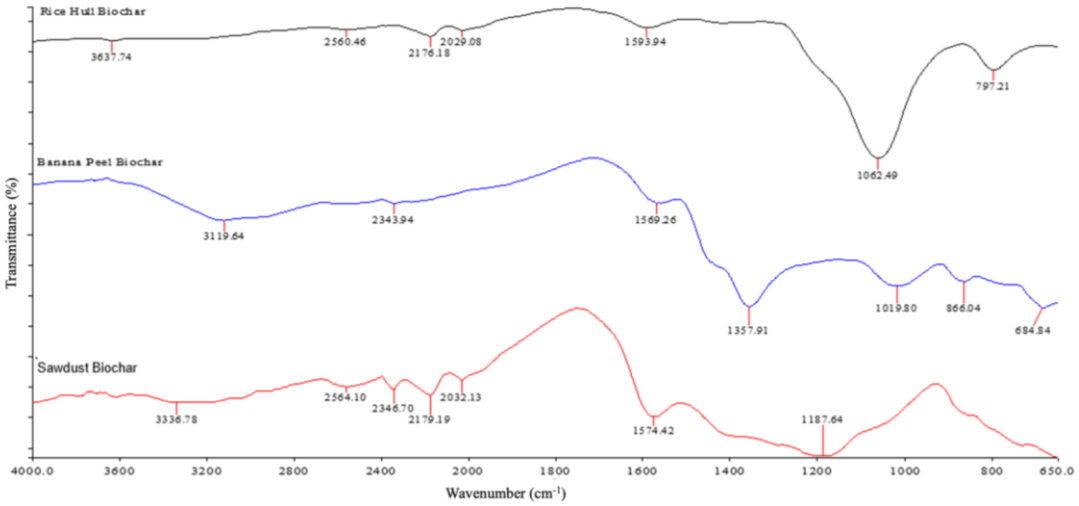

Figure 4. FTIR spectra of each biochar.

Table 2. Major functional groups of feedstocks classified by FTIR spectra.

Range of wavenumber (cm^{-1})	Wavenumber of feedstocks (cm^{-1})			Functional groups	Classification of compounds
	Rice Hull	Banana Peel	Sawdust		
3500 – 3000	3318.38	3309.64	3334.90	O-H stretching	Alcohol
				C-H stretching	Alkyne
				N-H stretching	Amines
3000 – 2800	2921.68	2925.65	2918.04	O-H stretching	Carboxylic acid, alcohol
				N-H stretching	Amine salt
2800 – 2500	2545.74	-	2554.82	O-H stretching	Carboxylic acid
2500 - 2300	2348.55	2347.01	2346.68	O=C=O stretching	Carbon dioxide
2300 – 2100	2174.00	2173.57	2175.27	S-C≡N stretching	Thiocyanate
2100 – 2000	2027.49	2024.00	2027.76	N=C=S stretching	Isothiocyanate
1800 – 1700	-	1719.87	-	C=O stretching	Carboxylic acid, aliphatic ketone, unsaturated ester
1700 – 1500	1642.00	1610.29	1596.04	C=N stretching	Imine/oxime
				N-H stretching	Amine
				C=C stretching	Cyclic alkene
1500 – 1400	-	1443.55	1444.61	C-H bending	Alkene
1400 - 1300	-	1361.12 - 1305.14	1334.49	N-O stretching	Nitro compound
				O-H bending	Alcohol, phenol
				C-F stretching	Fluoro compound
				C-N stretching	Aromatic amine
				S=O stretching	Sulfone
				C=O stretching	Aromatic ester
1300 - 1000	1030.14	1029.01	1233.69 - 1029.21	C-O stretching	Alkyl aryl ether, vinyl ether
				C-N stretching	Amine
				C-F stretching	Fluoro compound
				S=O stretching	Sulfoxide

Reduction of moisture content, OM combustion, and mineral content of the samples could result in the variation of FTIR spectra [28]. This might have happened as a result of aromatic hydrocarbons in biochar breaking and reforming [29]. The broad bands at 3318.38 cm^{-1} (rice hull feedstock), 3309.64 cm^{-1} (banana peel feedstock), 3334.90 cm^{-1} (sawdust feedstock), 3637.74 cm^{-1} (RHB-500), 3119.64 cm^{-1} (BPB-550) and 3336.78 cm^{-1} (SDB-500) indicated the presence of O-H stretching of alcohol and carboxylic acid group [30]. The intensity of transmittance peaks for all the biochars became lower, and the peak of biochars was broadened compared to the feedstocks. It means that the amount of O-H functional group was being reduced due to the pyrolysis process [31]. Similar research was done by Lam *et al.*

(2016) [32], where banana peel feedstock showed the highest transmittance compared to other feedstocks. It means that banana peel probably has the highest oxygen content among the feedstocks [32]. By referring to the Infrared Spectroscopy Absorption Table by Davis (2014) [33], all biochars showed the presence of O-H stretching for carboxylic acid and alcohol group at the bands of 2925.65 – 2918.04 cm^{-1}, N-H bending for amine and C=C stretching for cyclic alkene at bands of 1593.94 – 1574.42 cm^{-1}. The Si-O-Si group was perceived in RHB-500 at 1040 – 1100 cm^{-1} [33]. Si-O-Si is a core constituent in the chemical structure of rice hull as silica prevents the decomposition of plant carbon [34].

Table 3. Major functional groups of biochars classified by FTIR spectra.

Range of wavenumber (cm^{-1})	Wavenumber of biochars (cm^{-1})			Functional groups	Classification of compounds
	Rice Hull (RHB-500)	Banana Peel (BPB-550)	Sawdust (SDB-500)		
3700 - 3000	3637.74	3119.64	3336.78	O-H stretching	Alcohol, carboxylic acid
				N-H stretching	Aliphatic primary amine, secondary amine
2600 – 2500	2560.46	-	2564.10	O-H stretching	Carboxylic acid
				S-H stretching	Thiol
2400 – 2300	-	2343.94	2346.70	O=C=O stretching	Carbon dioxide
2200 – 2000	2029.08	-	2179.19 – 2032.13	S-C≡N stretching	Thiocyanate
				N=C=S stretching	Isothiocyanate
1600 – 1500	1593.94	1569.26	1574.42	N-H bending	Amine
				C=C stretching	Cyclic alkene
1400 – 1300	-	1357.91	-	O-H bending	Alcohol, phenol
				N-O stretching	Nitro compound
				S=O stretching	Sulfonate, sulfonamide
1200 – 1100	-	-	1187.64	C-O stretching	Ester, tertiary alcohol
				S=O stretching	Sulfate, sulfonyl chloride, sulfonate
				C-F stretching	Fluoro compound
1100 – 1000	1062.49	1019.80	-	C-O stretching	Alkyl aryl ether, vinyl ether, primary alcohol
				C-N stretching	Amine
				S=O stretching	Sulfoxide
				Si-O-Si	Organic siloxane or silicone
900 - 600	797.21	866.04 – 684.84	-	C-H bending	Alkanes, alkynes
				C=C bending	Alkene
				C-Br bending	Halo compound
				N-H wagging	Amines, secondary amides
				N-O stretching	Nitro compound

In general, all samples were majority showing the functional group of the oxygenated-functional group, which are alcohol, phenol, carboxylic acid, and aliphatic functional groups like alkane and alkene. There is only a small amount of aldehydes and ketones were identified. From the spectra obtained, banana peel and sawdust feedstocks presented the presence of a C=O stretching bond, but this bond disappeared after the pyrolysis. This disappearance is due to the hydrogenation reaction that occurred during the pyrolysis. Hydrogenation could lead to the extinguishment of aldehyde and ketone to aromatic bond, C-O and C-C aliphatic to ketone, and C-O aliphatic bond to the aromatic correlation [35]. Therefore, the disappearance of the C=O stretching bond denoted that the reaction between aldehyde/ketone and other functional groups is high during the hydrogenation.

3.3. Morphology.

Figure 5 shows the SEM images of three different feedstocks and biochars under the magnifications of 1000x. Overall, all biochars and sawdust feedstock had a smoother surface compared to the feedstocks. Another two feedstocks, rice hull and banana peel, were observed

to have a rough and uneven surface. The samples have different structures and surfaces due to the grinding and sieving process applied to the samples [36].

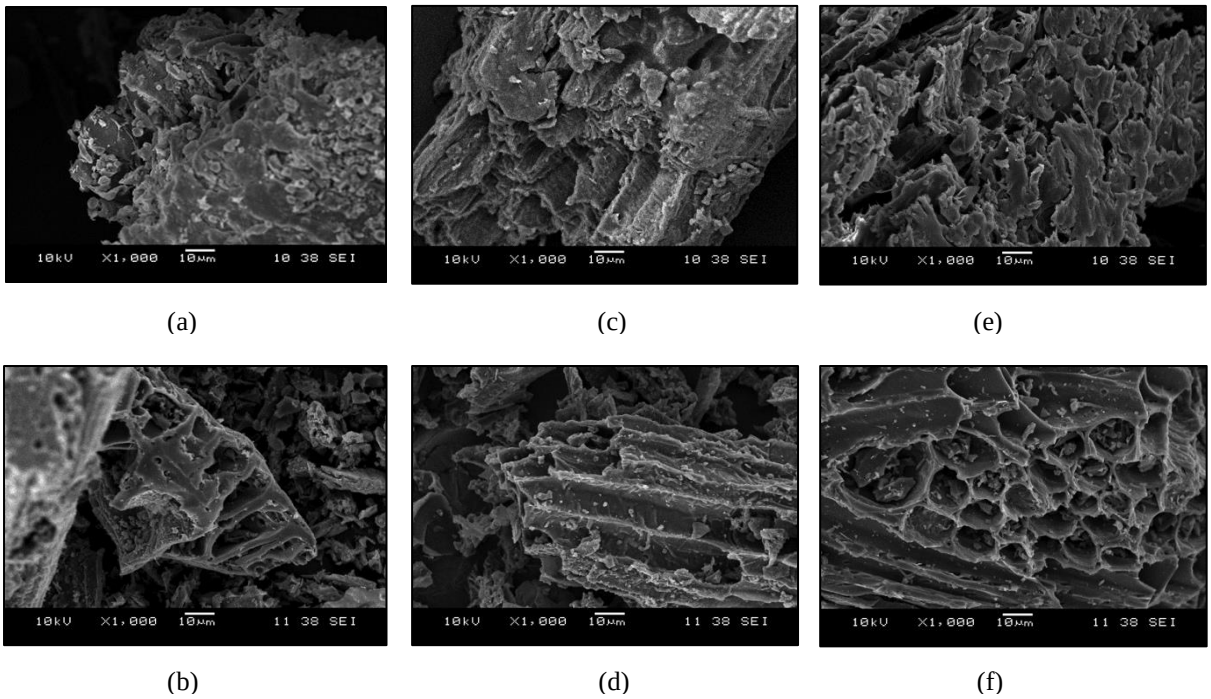

(a) (c) (e)

(b) (d) (f)

Figure 5. Scanning Electron Microscopy (SEM) images of rice hull feedstock (a) and RHB-500 (b), banana peel feedstock (c) and BPB-550 (d), sawdust feedstock (e), and SDB-500 (f).

RHB-500 showed some broken hollows with poor uniformity of pore structure. SDB-500 had a honeycomb surface with a visible layered structure. BPB-550 showed a longitudinal structure that may be attributed to the fibrous content of banana peel. From the observation, three types of biochars showed pore formation, as shown in Figure 5 (b), (d), and (f). However, SEM images for the three feedstocks in Figure 5 (a), (c), and (e) did not clearly show the pore formation compared to the biochars. All biochars possessed micropores with a size below 30 μm. The average pore size of rice hull, banana peel, and sawdust feedstock are 2.7 μm, 12.2 μm, and 7.6 μm, respectively, while each biochar showed the pore size of 21.3 μm, 13.8 μm, 13.7 μm, respectively.

In removing H_2S from porous materials, surface functionality and porosity are critical. As the pyrolysis process is undergoing, the thermal decomposition will cause the vaporization of volatile matter contained in the feedstocks and create a space among the pores [11,17]. Thus, the formation of different pore sizes with a small amount is due to the dehydration and vaporization of biochars. The results indicated that the number of pores increased after the pyrolysis. Porous materials, like activated carbons, are commonly employed as sorbents because of their porous properties, ideal for capturing H_2S [37,38].

3.4. Synthesis of hydrogen sulfide (H_2S).

The concentration of H_2S was monitored for 8 days. Figure 6 demonstrated that 4 ppm of H2S was produced on the second day after the MSW was added to the column. The concentration of H_2S was then increased gradually until the concentration reached the peak of 221 ppm on the fifth day. However, the concentration of H_2S started to drop starting the fifth day. The concentration dropped until 7 ppm on the eighth day. The adsorption of H_2S can also be influenced by biogas-related molecules such as CO_2 and CH_4 [39,40]. The reduction of H_2S

concentration after the peak value is due to the lacking of organic carbon source and consequently resulted in the inactivity of sulfate-reducing bacteria (SRB) found in the MSW [41-43].

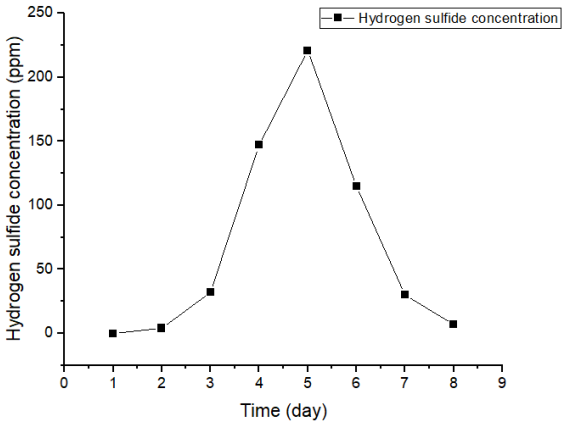

Figure 6. Graph of H_2S concentration versus day.

3.5. Adsorption of hydrogen sulfide (H_2S).

Generally, the three biochars, which are RHB-500, BPB-550, and SDB-500, had the ability to reduce the H_2S from the MSW. According to Figure 7, the removal efficiency of H_2S showed the peak value of 94.71%, 98.23%, and 95.03% using RHB-500, BPB-550, and SDB-500, respectively. Therefore, employing biochars as an adsorbent, removing H_2S from a combination of gases in odorous gas from MSW [44].

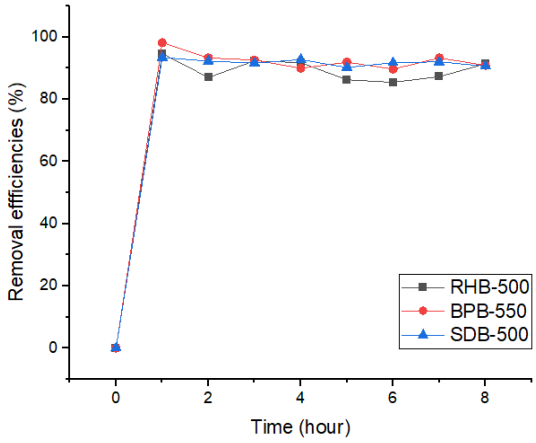

Figure 7. The removal efficiency of H_2S among three different biochars.

The mechanism is shown as below:

$$H_sS_{gas} \xrightarrow{K_H} H_2S_{ads} \quad (1)$$

$$H_sS_{ads} \xrightarrow{K_S} H_2S_{ads.liq} \quad (2)$$

$$H_2S_{ads.liq} \xrightarrow{K_a} HS^-{}_{ads} + H^+ \quad (3)$$

$$HS^-{}_{ads} + 3O^*{}_{ads} \xrightarrow{K_{R1}} SO_{2_{ads}} + OH^- \quad (4)$$

$$SO_{2_{ads}} + O^{*ads} + H_2O_{ads} \xrightarrow{K_{R2}} H_2SO_{4_{ads}} \quad (5)$$

$$H^+ + OH^- \rightarrow H_2O \quad (6)$$

It started with the H_2S adsorption on the biochar surface occurs as shown in Equation 1. Then H_2S dissolution in the water film will form $H_2S_{ads,liq}$ (Equation 2), followed by

dissociation of the adsorbed phase of H_2S in the water film (Equation 3). The surface of H_2S ion (HS^-) at adsorbed state that formed in the previous equation will then react with dissociative adsorbed oxygen, which is O^*_{ads}. The reaction leads to the formation of sulfur dioxide (SO_2) (Equation 4). Further oxidation of SO_2 is causing the production of sulphuric acid (H_2SO_4) with the existence of water (H_2O) (Eq. 5). H_2S in gas, adsorbed, and liquid phases are represented by the terms of H_2S_{gas}, $H_2S_{ads,}$ and $H_2S_{ads,liq,}$ respectively. As the order for the removal efficiency was BPB-550 > SDB-500 > RHB-500, the order for pH level among the three biochars was also the same. Adsorption will occur when the acidic H_2S has contact with biochars surface, which is alkaline [45]. As the pH of biochar is higher, the dissociation of H_2S will be enhanced, and thus the oxidation of H_2S to sulfur will be altered [9,24,46]. The pH of the BPB-550 is the highest among the three biochars, yet it has the highest removal efficiency of H_2S. It can be concluded that a higher pH level will lead to the higher removal efficiency of H_2S [9,47].

4. Conclusions

This study was conducted to produce and investigate the characteristics of biochars derived from rice hull, banana peel, and sawdust. Alkalinity could enhance the removal ability of H_2S. This study showed that as pyrolysis temperature was increased from 400 ^{0}C to 600°C, the alkalinity of biochars increased. All biochars produced were alkaline, and BPB-550 had the pH value of 10.06, which is the highest. However, the percentage of biochar yield decreased with increased pyrolysis temperature resulting from the increase in lignin and hemicellulose thermal decomposition. Among the three different biochars, RHB-500 gave the highest biochar yield. The pH level of biochars acted as the indicator to fix the pyrolysis temperature for further characteristics of each biochar. Rice hull biochars (RHB-500) and sawdust biochars (SDB-500) were fixed at the pyrolysis temperature of 500°C while banana peel biochars (BPB-550) was fixed at 550°C. SDB-500 possessed the lowest ash content in this study. In addition, all feedstocks revealed the bands at the range of 3318.38 cm^{-1} to 1029.01 cm^{-1} with the presence of O-H stretching, N-H stretching, C=C stretching, C-O stretching, and C-N stretching functional group. On the other hand, the wavenumber of biochars was between 3637.74 cm^{-1} to 684.84 cm-1. All three biochars produced have been found to have the surface functional group of O-H stretching, N-H bending and C=C stretching. Significant changes in the surface morphology and pore size before and after the pyrolysis process of biochars were shown. The pores formation became more obvious, and the pore size increased after the pyrolysis due to the dehydration and vaporization of biochars. The concentration of synthetic H_2S reached the peak concentration of 221 ppm on the fifth day. The order for the removal efficiency is BPB-550 (98.23%) > SDB-500 (95.03%) > RHB-500 (94.71%). Higher pH could enhance the dissociation of H_2S, which could also help improve the removal efficiency of H_2S by biochars. Overall, the biochars had a strong ability to act as the adsorbents for H_2S removal. This research utilized biochars derived from agricultural waste to reduce H_2S. It is recommended to investigate the optimum pyrolysis temperature, heating rate, and pH of biochars should be determined to produce the desired properties of biochars in order to achieve higher efficiency in removing H_2S. Different biochars derived from other biomass waste should also be studied and compared. Besides that, Thermogravimetric Analysis (TGA), CHNS/O elemental analysis, and specific surface area (SSA) by using Brunauer-Emmett-Teller (BET) method are recommended to be studied. A larger surface area might enhance the adsorption potential, and therefore, a wide range of biochars characterization should be done to study their various effects on the removal efficiency of H_2S.

Funding

This research was supported by Universiti Malaysia Perlis, Malaysia, under the Research Materials Fund (RESMATE)-9001-00624.

Acknowledgments

The authors would like to acknowledge the technical assistants of the Faculty of Civil Engineering Technology, Universiti Malaysia Perlis.

Conflicts of Interest

The authors declare no conflicts of interest.

References

1. Okoro, O.V.; Sun, Z. Desulphurisation of biogas: a systematic qualitative and economic-based quantitative review of alternative strategies. *Chem Eng* **2019**, *3*, https://doi.org/10.3390/chemengineering3030076.
2. Ali, I.; Asim, M.; Khan, T.A. Low cost adsorbents for the removal of organic pollutants from wastewater. *J Environ Manage* **2012**, *113*, 170–183, http://doi.org/10.1016/j.jenvman.2012.08.028.
3. Amvrosios, G.G.; Nikolaos, C.; Ioannis, V.Y.; Maria, A.G. Hydrogen sulfide (H_2S) removal via MOFs. *Materials* **2020**, *13*, https://doi.org/10.3390/ma13163640.
4. Crombie, K.; Mašek, O.; Sohi, S.P.; Brownsort, P.; Cross; A. The effect of pyrolysis conditions on biochar stability as determined by three methods. *GCB Bioenergy* **2013**, *5*, 122–131, http://doi.org/10.1111/gcbb.12030.
5. Hyung, J.; Chul, H.; Jin, D. Pyrolysis of seaweeds for bio-oil and bio-char production. *Chem Eng Trans* **2014**, *37*, 121–126, http://doi.org/10.3303/CET1437021.
6. Zeng, B.; Shimizu, N. Hydrogen generation from wood chip and biochar by combined continuous pyrolysis and hydrothermal gasification. *Energies* **2021**, *14*, https://doi.org/10.3390/en14133793.
7. Liang, H.; Chen, L.; Liu, G.; Zheng, H. Surface morphology properties of biochars produced from different feedstocks. *Iccte* **2016**, 1205–1208, https://doi.org/10.2991/iccte-16.2016.210.
8. Abdullah, N.; Sulaiman, F.; Miskam, M.A.; Taib, R.M. Characterization of banana (Musa spp .) pseudostem and fruit-bunch-stem as a potential renewable energy resource. *International Journal of Biological, Veterinary, Agricultural and Food Engineering* **2014**, *8*, 815–819.
9. Shang, G.; Shen, G.; Liu, L.; Chen, Q.; Xu, Z. Kinetics and mechanisms of hydrogen sulfide adsorption by biochars. *Bioresour Technol* **2013**, *133*, 495–499, http://doi.org/10.1016/j.biortech.2013.01.114.
10. Xu, X.; Cao, X.; Zhao, L. Comparison of rice husk- and dairy manure-derived biochars for simultaneously removing heavy metals from aqueous solutions: Role of mineral components in biochars. *Chemosphere* **2013**, *92*, 955–961, http://doi.org/10.1016/j.chemosphere.2013.03.009.
11. Khabazipour, M.; Anbia, M. Removal of hydrogen sulfide from gas streams using porous materials: a review. *Ind Eng Chem Res* **2019**, *58*, 22133–22164, https://doi.org/10.1021/acs.iecr.9b03800.
12. Chen, F.E.; Mandel, R.M.; Woods, J.J.; Lee, J.-H.; Kim, J.; Hsu, J.H.; Fuentes-Rivera, J.J.; Wilson, J.J.; Milner, P.J. Biocompatible metal–organic frameworks for the storage and therapeutic delivery of hydrogen sulfide. *Chem Sci* **2021**, *12*, 7848-7857, https://doi.org/10.1039/d1sc00691f.
13. Johari, A.; Ahmed, S.I.; Hashim, H.; Alkali, H.; Ramli, M. Economic and environmental benefits of landfill gas from municipal solid waste in Malaysia. *Renew Sustain Energy Rev* **2012**, *16*, 2907–2912, http://doi.org/10.1016/j.rser.2012.02.005.
14. Martínez-Ahumada, E.; Díaz-Ramírez, M.L.; Velásquez-Hernández, M.D.J.; Jancik, V.; Ibarra, I.A. Capture of toxic gases in MOFs: SO2, H_2S, NH3 and NOx. *Chem Sci* **2021**, *12*, https://doi.org/10.1039/D1SC01609A.
15. Major, J. Guidelines on practical aspects of biochar application to field soil in various soil management systems. *International Biochar Initiative* **2010**, *23*.
16. Zulkefli, N.N.; Masdar, M.S.; Wan-Isahak, W.N.R.; Abu-Bakar, S.N.H.; Abu-Hasan, H.; Mohd-Sofian, N. Application of response surface methodology for preparation of ZnAC2/CAC adsorbents for hydrogen sulfide (H_2S) capture. *Catalysts* **2021**, *11*, https://doi.org/10.3390/catal11050545.
17. Aziz, N.S.; Nor, M.A.; Manaf, S.F.; Hamzah, F. Suitability of biochar produced from biomass waste as soil amendment. *Procedia-Social and Behavioral Sciences* **2015**, *195*, 2457–2465, http://doi.org/10.1016/j.sbspro.2015.06.288.
18. Karim, A.; Manish, K.; Sanghamitra, M.S. Banana peduncle biochar: characteristics and adsorption of hexavalent chromium from aqueous solution. *Int Res J Pure Appl Chem* **2015**, *7*, 1–10,

http://doi.org/10.9734/IRJPAC/2015/16163.
19. Barrera, E.; Cajero, P. Characterization of lignocellulosic fruit waste as an alternative feedstock for bioethanol production. *BioResources* **2014**, *9*, 1873–1885, http://dx.doi.org/10.15376/biores.9.2.1873-1885.
20. Ahmad, M.; Lee, S.S.; Dou, X.; Mohan, D.; Sung, J.K.; Yang, J.E.; Ok, Y.S. Effects of pyrolysis temperature on soybean stover- and peanut shell-derived biochar properties and TCE adsorption in water. *Bioresour Technol* **2012**, *118*, 536–544. http://doi.org/10.1016/j.biortech.2012.05.042.
21. Carrasco, B.; Ávila, E.; Viloria, A.; Ricaurte, M. Shrinking-core model integrating to the fluid-dynamic analysis of fixed-bed adsorption towers for H2S removal from natural gas. *Energies* **2021**, *14*, https://doi.org/10.3390/en14175576.
22. Saletnik, B.; Bajcar, M.; Saletnik, A.; Zaguła, G.; Puchalski, C. Effect of the pyrolysis process applied to waste branches biomass from fruit trees on the calorific value of the biochar and dust explosivity. *Energies* **2021**, *14*, https://doi.org/10.3390/en14164898.
23. Satoshi, A.; Hiroyuki, S.; Tsuyoshi, I.; Shinjiro, H.; Takahito, O. Removal of hydrogen sulfide gas using coal fly ash – blast furnace cement composite. *J Water Sanit Hyg Dev* **2021**, *11*, 824-830, https://doi.org/10.2166/washdev.2021.091.
24. Xu, X.; Cao, X.; Zhao, L.; Sun, T. Comparison of sewage sludge- and pig manure-derived biochars for hydrogen sulfide removal. *Chemosphere* **2014**, *111*, 296–303, http://doi.org/10.1016/j.chemosphere.2014.04.014.
25. Hernandez-Mena, L.E.; Pecora, A.B.; Beraldo, A.L. Slow pyrolysis of bamboo biomass: Analysis of biochar properties. *Chem Eng Trans* **2014**, *37*, 115–120, http://doi.org/10.3303/CET1437020.
26. Stella-Mary, G.; Sugumaran, P.; Niveditha, S.; Ramalakshmi, B.; Ravichandran, P.; Seshadri, S. Production, characterization and evaluation of biochar from pod (Pisum sativum), leaf (Brassica oleracea) and peel (Citrus sinensis) wastes. *Int J Recycl Org Waste Agric* **2016**, *5*, 43–53, http://doi.org/10.1007/s40093-016-0116-8.
27. Mofijur, M.; Mahlia, T.M.I.; Logeswaran, J.; Anwar, M.; Silitonga, A.S.; Ashrafur-Rahman, S.M.; Shamsuddin, A.H. Potential of rice industry biomass as a renewable energy source. *Energies* **2019**, *12*, 4116, http://doi.org/10.3390/en12214116.
28. Cao, X.; Harris, W. Properties of dairy-manure-derived biochar pertinent to its potential use in remediation. *Bioresour Technol* **2010**, *101*, 5222–5228, http://doi.org/10.1016/j.biortech.2010.02.052.
29. Lithnes, K.P.; Li, W.Y.; Wai, Y.W.; Siek, T.Y.; Ming, M.P. Application of biochar derived from different types of biomass and treatment methods as a fuel source for direct carbon fuel cells. *Energies* **2019**, *12*, https://doi.org/10.3390/en12132477.
30. Coates, J. Interpretation of infrared spectra, a practical approach. *Encyclopedia of Analytical Chemistry* **2000**, 10815–10837.
31. Mohammed, I.Y.; Abakr, Y.A.; Kazi, F.K.; Yusuf, S.; Alshareef, I.; Chin, S.A. Pyrolysis of Napier grass in a fixed bed reactor : effect of operating conditions on product yields. *Bioresources* **2015**, *10*, 6457–6478, http://doi.org/10.15376/biores.10.4.6457-6478.
32. Lam, S.S.; Liew, R.K.; Lim, X.Y.; Ani, F.N.; Jusoh, A. Fruit waste as feedstock for recovery by pyrolysis technique. *Int Biodeterior Biodegradation* **2016**, *113*, 325–333, http://doi.org/10.1016/j.ibiod.2016.02.021.
33. Davis, U. *Infrared spectroscopy absorption table*. The Chemistry LibreTexts Library, **2014**; pp. 1-4.
34. Jindo, K.; Mizumoto, H.; Sawada, Y.; Sanchez-Monedero, M.A.; Sonoki, T. Physical and chemical characterization of biochars derived from different agricultural residues. *Biogeosciences* **2014**, *11*, 6613–6621, http://doi.org/10.5194/bg-11-6613-2014.
35. McClelland, D.J.; Motagamwala, A.H.; Li, Y.; Rover, M.R.; Wittrig, A.M.; Wu, C.; Buchanan, J.S.; Brown, R.C.; Ralph, J.; Dumesic, J.A.; Huber, G.W. Functionality and molecular weight distribution of red oak lignin before and after pyrolysis and hydrogenation. *Green Chemistry* **2017**, *19*, 1378-1389, http://doi.org/10.1039/C6GC03515A.
36. Hwidi, R.S.; Tengku-Izhar, T.N.; Mohd-Saad, F.N. Characterization of limestones as raw material to hydrated lime. *E3S Web of Conferences* **2018,** *34*, https://doi.org/10.1051/e3sconf/20183402042.
37. Liang, S.; Peng, B.; Liu, S.; Zhang, W.; Guo, M.; Cheng, F.; Zhang, M. Low-temperature highly efficient and selective removal of H_2S over three-dimensional Zn–Cu-based materials in an anaerobic environment. *Environ Sci Technol* **2020**, *54*, 5964–5972, https://doi.org/10.1021/acs.est.0c00503.
38. Yang, J.H. Hydrogen sulfide removal technology: A focused review on adsorption and catalytic oxidation. *Korean J Chem Eng* **2021**, *38*, 674–691, https://doi.org/10.1007/s11814-021-0755-y.
39. Amvrosios, G.G.; Nikolaos, D.C.; Maria, A.G. Removal of hydrogen sulfide from various industrial gases: a review of the most promising adsorbing materials. *Catalysts* **2020**, *10*, https://doi.org/10.3390/catal10050521.
40. Amvrosios, G.G.; Nikolaos, D.C.; Safa, G.; Kyriaki, P.; Ioannis, V.Y.; Maria, A.G. Adsorption of hydrogen sulfide at low temperatures using an industrial molecular sieve: an experimental and theoretical study. *ACS Omega* **2021**, *6*, 14774-14787, https://doi.org/10.1021/acsomega.0c06157.
41. Xu, Q.; Townsend, T.; Bitton, G. Inhibition of hydrogen sulfide generation from disposed gypsum drywall using chemical inhibitors. *J Hazard Mater* **2011**, *191*, 204–211,

http://doi.org/10.1016/j.biortech.2011.08.089.
42. Phyo, A.K.; Jia, Y.; Tan, Q.; Sun, H.; Liu, Y.; Dong, B.; Ruan, R. Competitive growth of sulfate-reducing bacteria with bioleaching acidophiles for bioremediation of heap bioleaching residue. *Int J Environ Res Public Health* **2020**, *17*, 2715. https://doi.org/10.3390/ijerph17082715.
43. Tran, T.T.T.; Kannoorpatti, K.; Padovan, A.; Thennadil, S. Sulphate-reducing bacteria's response to extreme pH Environments and the effect of their activities on microbial corrosion. *Appl Sci* **2021**, *11*, https://doi.org/10.3390/app11052201.
44. de-Oliveira, L.H.; Meneguin, J.G.; Pereira, M.V.; do-Nascimento, J.F.; Arroyo P.A. Adsorption of hydrogen sulfide, carbon dioxide, methane, and their mixtures on activated carbon. *Chem Eng Commun* **2019**, *206*, 1533-1553, https://doi.org/10.1080/00986445.2019.1601627.
45. Shang, G.; Li, Q.; Liu, L.; Chen, P.; Huang, X. Adsorption of hydrogen sulfide by biochars derived from pyrolysis of different agricultural forestry wastes. *J Air Waste Manage Assoc* **2016**, *66*, 8–16, http://doi.org/10.1080/10962247.2015.1094429.
46. Hsiu, W.O.; Ming, S.C.; Hsiao, Y.C. Removal of hydrogen sulfide from biogas using a bubbling tank fed with aerated wastewater. *Aerosol Air Qual Res* **2020**, *20*, 643–653, https://doi.org/10.4209/aaqr.2019.12.0647.
47. Joanna, K.H.; Lawrence, Q.; Amro, H.; Stephanie, L. Comparing hydrogen sulfide removal efficiency in a field-scale digester using microaeration and iron filters. *Energies* **2020**, *13*, https://doi.org/10.3390/en13184793.